IEEE Access
Multidisciplinary | Rapid Review | Open Access Journal

Received 8 May 2022, accepted 13 June 2022, date of publication 21 June 2022, date of current version 27 June 2022.

Digital Object Identifier 10.1109/ACCESS.2022.3185123

RIS Assisted Triple-Hop RF-FSO Convergent With UWOC System

L. BHARGAVA KUMAR[1], RAMAVATH PRASAD NAIK[2], PRABU KRISHNAN[1], (Senior Member, IEEE), A. AROCKIA BAZIL RAJ[3], (Member, IEEE), ARUN K. MAJUMDAR[4], (Life Member, IEEE), AND WAN-YOUNG CHUNG[5], (Senior Member, IEEE)

[1]Department of Electronics and Communication Engineering, National Institute of Technology Karnataka, Surathkal 575025, India
[2]Research Institute of Artificial Intelligence Convergence, Pukyong National University, Nam-gu, Busan 48513, Republic of Korea
[3]Department of Electronics Engineering, Defence Institute of Advanced Technology, Pune 411025, India
[4]Department of Electrical Engineering and Computer Science, University of Colorado, Pueblo, CO 81001, USA
[5]Department of Electronic Engineering, Pukyong National University, Nam-gu, Busan 48513, Republic of Korea

Corresponding authors: Wan-Young Chung (wychung@pknu.ac.kr) and Prabu Krishnan (prabuk@nitk.edu.in)

This work was supported by the Research Grant funded by the National Research Foundation (NRF) of Korea under Grant 2020R1A4A1019463.

ABSTRACT The convergence of wireless optical communication (WOC) and radio-frequency (RF) systems is a promising technology that overcomes the shortcomings of standalone communication systems. By incorporating reconfigurable intelligent surfaces (RISs) on top of these WOC and RF communication systems, it is possible to circumvent the connection challenges associated with standard line of sight (LOS) communication links. Wireless communication systems with RIS assistance are a promising and evolving technology that enables more efficient and reliable link performance over long distances. The performance of the triple-hop RIS-assisted RF-FSO convergent with the underwater wireless optical communication (UWOC) system is investigated in this article. We considered the fading channel Nakagami-m over the RIS-RF connection and the fading channel Gamma-Gamma (GG) over the RIS-FSO and UWOC links. Then, the average bit error rate (ABER) and outage probability are determined using closed-form expressions. The ABER and outage probability performances of the triple-hop communication system is analysed by varying parameters such as turbulence, misalignment fading, and the number of RIS elements. The obtained results demonstrate an improvement in performance for low turbulence, low pointing error, and an increasing number of RIS elements. Additionally, the data demonstrate the accuracy of the analytical results.

INDEX TERMS RIS, RF, FSO, UWOC, ABER.

I. INTRODUCTION

Recently, integrating radio frequency (RF) communications and wireless optical communication (Free-space optical (FSO) communication and underwater wireless optical communication (UWOC)) has become attractive. FSO communications have pros compared to RF communications regarding data transfer rate, massive bandwidth availability, cost-effectiveness, and license-free. Although this is interesting, the FSO communication system suffers from atmospheric turbulence and misalignment fading. Moreover, the other approaches, such as diversity, usage of adaptive modulation, error control coding, and aperture averaging, were proposed to overcome the effects mentioned earlier. Combining or converging the two different technologies will bring their pros, making the communication system efficient and exciting [1], [2].

Wireless communications and wireless optical communications (WOC) are entering a new era with the introduction of reconfigurable intelligent surfaces (RISs). RIS-assisted wireless communications are undergoing a revolution to empower an intelligent and reconfigurable radio/wireless optical environment for upcoming wireless communication systems. RISs are also known as large intelligent surfaces (LISs) or intelligent reflecting surfaces (IRSs). RIS is an artificial reflecting electromagnetic surface material that reflects, refracts, and scatter the received radio/optical signal and propagates it further, impacting its parameters such as phase,

The associate editor coordinating the review of this manuscript and approving it for publication was Jiajia Jiang.

frequency, amplitude, and polarization [3]. The RIS module's design depends on its application. The RIS module is an array of many mirrors that guide the received signal to a particular area of interest with their low power consumption. To design, the RIS modules require electronically controllable devices. These RIS modules solve problems in several zones where a radio/optical signal cannot propagate in the conventional line-of-sight (LOS) ways [4], [5]. Hence the RIS devices are applicable for RF, FSO, and unmanned aerial vehicle (UAV)-based wireless communication systems.

There has been a rapid growth in the implementation/use of convergent/hybrid/mixed/cooperative/relay-assisted wireless communication systems from the past five years. In [6], a RF-FSO convergent system was proposed and performances were studied. Similarly, the FSO/mmwave convergent systems are studied in [7]–[9], and co-operative RF-UWOC systems were studied and their average bit error rate (ABER) and outage probability performances were evaluated in [10]–[12], and the authors in [13]–[18] proposed FSO/UWOC systems and studied their ABER and outage performances. Experimental demonstration of various convergent systems are evolved in [19]–[22]. These convergent systems bring the advantages of individual communication systems and make the end-to-end system efficient.

Recently, authors in [23] performed a survey on RIS device principles and their applications in cellular networks beyond 5G, indoor communications, UAV-based systems for smart city, and intelligent IoT networks. Yang *et al.* investigated the performance of a RIS-assisted dual-hop UAV communication system in [24]. In the first hop, they considered the RIS to communicate with the UAV relay and a direct link used from the UAV to the destination. In [25], the authors presented and analyzed the potential benefits of adopting RISs for indoor and outdoor environments at various frequencies used for 6G and beyond wireless networks. The authors proposed and investigated an optical RIS-based controllable multi-branch WOC system by establishing multiple optical RISs in [26]. RIS-assisted dual-hop FSO-RF system was proposed for an outdoor environment and the authors have investigated its outage and BER performance in [27]. The relay converts the optical signal into an RF signal using either decode and forward (DF) protocol and is reflected to the user device using the RIS module. It is an FSO link in the first-hop, while the second-hop deploys an RF link using RIS. A RIS-based dual-hop mixed FSO-RF communication system was proposed and evaluated in [3] under co-channel interference (CCI). Li *et al.* proposed a RIS-assisted dual-hop RF-UWOC system and investigated its performance in [28].

Exploring the undersea world is a difficult endeavour due to the harsh communication features. Another difficulty in ocean monitoring applications is the transmission of gathered data to control stations at a high data rate. Individual RF, FSO, and UWOC systems each provide their own limitations and challenges. The constraints and limits of RF systems include limited bandwidth and FSO systems, which restrict LOS communication. Therefore, the converging triple hop RF-FSO-UWOC system with the well-developed RIS facilitates further underwater exploration and facilitates the transmission of ocean data to the control stations. This motivated us towards the development of a RIS-assisted triple-hop communication system.

The contributions of this paper are as follows:

- We proposed a triple-hop RIS-assisted RF-FSO convergent with UWOC system for the first time.
- The ABER and outage performance of the proposed system are evaluated using the close-form expressions.
- The performance evaluation of the trip-hop system is made for varying number of reflecting elements on RIS over FSO link.
- Turbulence and misalignment fading parameters of FSO link are varied in order to analyze the performance of the end-to-end system.

Section II gives the details of the system model. Section III presents channel models for the RF, FSO, and UWOC links. Section IV provides the average bit error rate equations for each link and end-to-end system. Also outage probability equations are given for triple-hop system. Section V reviews the results and discussions. This paper concludes with future work directions in Section VI.

II. SYSTEM MODEL

We considered a triple-hop wireless communication system as shown in Figure 1. We use a RIS-RF system for the first hop, a RIS-FSO system for the second hop, and the third hop uses the UWOC system. The source is a base station that connects to the lighthouse (relay-1) through RIS placed on a building as direct communication to relay-1 is impossible. Similarly, relay-1 connects to the ship (relay-2) through RIS-assisted buoy as LOS communication does not work. The underwater wireless autonomous vehicles (UWAVs) directly communicate with the ship.

The light beam reflects specularly with the help of simple mirrors or perfect smooth surfaces in FSO systems (Snell's law of reflection), making the scattering negligible. Optical RIS elements are made up of using the smart mirrors of very small size (depending on the optical wavelengths, order of nano-meters); initially, lenses at the source are adjusted to occupy the optical beam available N_{FSO} RIS elements. [29]–[31].

III. STATISTICAL CHARACTERISTICS

A. CHANNEL MODEL

1) RF LINK

The maximized electrical SNR of an RIS-assisted RF link can be given as

$$\gamma_1 = \sum_{i=1}^{N_{RF}} (x_i\, y_i)^2\, \frac{P_s}{N_0} = \sum_{i=1}^{N_{RF}} Z_i^2\, \bar{\gamma}_1 \tag{1}$$

Here x_i and y_i are the two independent random variables and Nakagami-m distributed, P_s is the transmitted signal's average power, N_0 is variance of additive white Gaussian

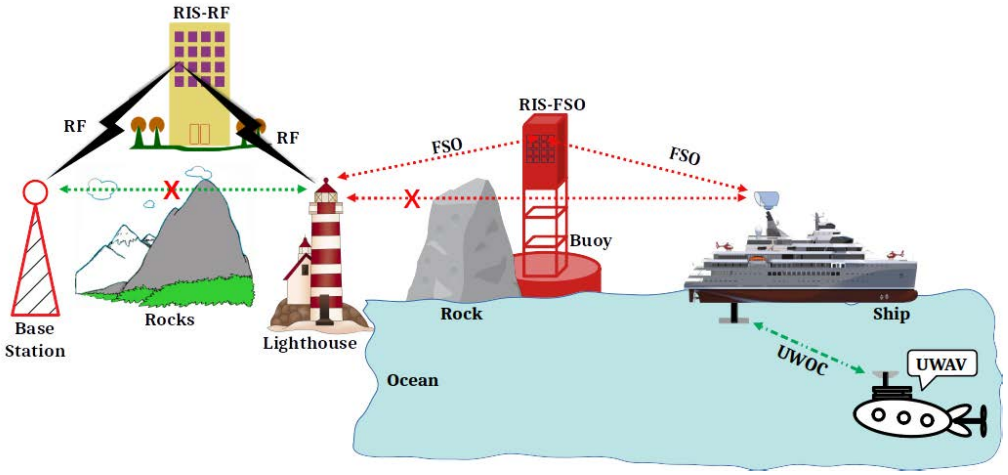

FIGURE 1. System model.

noise, N_{RF} is the number of reflecting elements on the RIS and $\bar{\gamma}_1$ is the average SNR of the RF link. $Z_i = x_i \cdot y_i$ is the product of two Nakagami-m random variables. The PDF of the new random variable Z_i is given as

$$f_{Z_i}(z) = \frac{4}{\Gamma(m)^2} \left(\frac{m}{\Omega}\right)^{2m} z^{2m-1} K_0\left(\frac{2mz}{\Omega}\right) \tag{2}$$

where $K_\nu(\cdot)$ is the ν-order modified Bessel function of the second kind, $m \in [1, 2, \cdots, \infty)$ is fading severity parameter and Ω is mean fading power. The mean and variance of Z_i are given as

$$E(Z_i) = \frac{m\Omega\Gamma(m+0.5)^2}{\Gamma(m+1)^2}$$

and

$$Var(Z_i) = \Omega^2 - \Omega^2 \frac{\Gamma(m+0.5)^4}{m^2\Gamma(m)^4}$$

where $\Gamma(\cdot)$ is Gamma function. Using the Laguerre expansion's first term, the PDF of the Nakagami-m distributed RF link in-terms of $Z = \sum_{i=1}^{N_{RF}} Z_i$ is given as

$$f_Z(z) = \frac{z^a}{\Gamma(a+1)\, b^{(a+1)}} \exp\left(-\frac{z}{b}\right) \tag{3}$$

where a and b are the mean and variance of Z, respectively, and given as,

$$a = \frac{\Gamma(m+0.5)^4(N_{RF}+1) - \Gamma(m)^4 m^2}{\Gamma(m)^4 m^2 - \Gamma(m+0.5)^4}$$

and

$$b = m\Omega\left(\frac{\Gamma(m)^2\Gamma(m+1)^2 - \Gamma(m+0.5)^4}{\Gamma(m+0.5)^2\Gamma(m+1)^2}\right).$$

Using the simple random variable transformation, the PDF of the instantaneous SNR (γ_1) for the product of two Nakagami-m random variables can be expressed as [32]

$$f_{\gamma_1}(\gamma_1) \simeq \frac{\gamma_1^{\frac{a-1}{2}}}{2\,(\bar{\gamma}_1)^{\frac{a+1}{2}}\, b^{(a+1)}\, \Gamma(a+1)} \exp\left(-\frac{\sqrt{\gamma_1}}{b\sqrt{\bar{\gamma}_1}}\right) \tag{4}$$

The CDF of Eq. (4) can be obtained as

$$F_{\gamma_1}(\gamma_1) \simeq \frac{\gamma\left(a+1, \sqrt{\frac{\gamma_1}{\bar{\gamma}_1}}\right)}{\Gamma(a+1)} \tag{5}$$

here $\gamma(\cdot,\cdot)$ is the lower incomplete Gamma function (Eq. (8.4.16.1)) given in [33]. By replacing the lower incomplete Gamma function with Meijer-G function, the CDF of Eq.(4) can be rewritten as

$$F_{\gamma_1}(\gamma_1) \simeq \frac{1}{\Gamma(a+1)} \mathrm{G}_{1,2}^{1,1}\left[\begin{matrix}1\\ a+1,0\end{matrix}\middle|\frac{1}{b}\sqrt{\frac{\gamma_1}{\bar{\gamma}_1}}\right] \tag{6}$$

2) FSO LINK

The electrical SNR of the RIS-assisted FSO link is given by

$$\gamma_2 = \sum_{j=1}^{N_{FSO}} u_j^2 \frac{P_r}{N_0} = B\bar{\gamma}_2 \tag{7}$$

where u_j is the j-th channel gain, P_r is the average power of the transmitted signal and $\bar{\gamma}_2$ is the average SNR of the FSO link. The FSO link Gamma-Gamma (GG) distributed under the atmospheric turbulence and a pointing error model caused by intelligent channel reconfigurable node (ICRN) jitter and beam jitter. The ICRN jitter caused by the jitter of the ICRN surface and the beam jitter is due to the jitter of the transmitter. The PDF of the FSO link (by assuming $B = u_j^2$) is given as [5]

$$f_B(h) = \frac{g\alpha\beta}{2A_0\sqrt{h}\,\Gamma(\alpha)\Gamma(\beta)} \mathrm{G}_{1,3}^{3,0}\left[\begin{matrix}g\\ g-1,\alpha-1,\beta-1\end{matrix}\middle|\frac{\alpha\beta}{A_0}\sqrt{h}\right] \tag{8}$$

where, α and β are the large scale and small scale turbulence parameters dependent on the scintillation index σ_R^2 expressed in Eqs. (9) and (10). Pointing error parameter is given as $g = \frac{W_{Z_{eq}}^2}{4\sigma_\theta^2 L^2 + 16\sigma_\beta^2 L_2^2}$, $W_{Z_{eq}} = w_z^2 \frac{erf(v)\sqrt{\pi}}{2ve^{-v^2}}$ denotes the error function and w_z is the beam-width, $A_0 = erf^2(v)$, $v = \frac{a_r}{w_z}\sqrt{\frac{\pi}{2}}$ denotes the aperture radius to beam width ratio, L is link-range from source to destination, L_2 is link-range from

RIS to destination, σ_θ and σ_β are standard deviations of pointing error and deflection error angle for ICRN jitter, respectively.

$$\alpha = \left[\exp\left(\frac{0.49\sigma_R^2}{\left(1 + 1.11\sigma_R^{12/5}\right)^{7/6}} \right) - 1 \right]^{-1} \tag{9}$$

and

$$\beta = \left[\exp\left(\frac{0.51\sigma_R^2}{\left(1 + 0.69\sigma_R^{12/5}\right)^{5/6}} \right) - 1 \right]^{-1} \tag{10}$$

here $\sigma_R^2 = 1.23\, C_n^2 k_w^{7/6} L^{11/6}$ is the Rytov variance, C_n^2 is the refractive index structure constant, $k_w = 2\pi/\lambda$ is the optical wave number, λ is the source wavelength.

The mean and variance of B can be obtained using

$$\mu_1 = E(B) = \frac{gA_0^2\,\Gamma(\alpha+2)\Gamma(\beta+2)\Gamma(g+2)}{\alpha^2\beta^2\,\Gamma(\alpha)\Gamma(\beta)\Gamma(g+3)} \tag{11}$$

and

$$\sigma_2^2 = Var(B) = \frac{gA_0^4\,\Gamma(\alpha+4)\Gamma(\beta+4)\Gamma(g+4)}{\alpha^4\beta^4\,\Gamma(\alpha)\Gamma(\beta)\Gamma(g+5)} - \mu_1^2 \tag{12}$$

Using the simple random variable transformation, the PDF of the Eq. (8) can be rewritten in terms of SNR as [5]

$$f_{\gamma_2}(\gamma_2) = \frac{g\alpha\beta}{2A_0\sqrt{\gamma_2\bar{\gamma}_2}\,\Gamma(\alpha)\Gamma(\beta)} \times \mathrm{G}_{1,3}^{3,0}\left[{}^{g}_{g-1,\alpha-1,\beta-1} \middle| \frac{\alpha\beta}{A_0}\sqrt{\frac{\gamma_2}{\bar{\gamma}_2}} \right]. \tag{13}$$

By using the central limit theorem, and assuming the large number of elements on RIS-FSO (i.e., N_{FSO}) and considering $\mu = \mu_1 N_{FSO}$, $\sigma^2 = \sigma_2^2 N_{FSO}$, the Eq. (13) can be rewritten as

$$f_{\gamma_2}(\gamma_2) \approx \frac{1}{\bar{\gamma}_2\sqrt{2\pi\sigma^2}} \exp\left(-\frac{(\gamma_2 - \bar{\gamma}_2\mu)^2}{2\sigma^2\bar{\gamma}_2^2} \right). \tag{14}$$

Using the simple mathematical calculations and the Eq.(1.211.1) of [34] the cumulative distribution function (CDF) of the Eq. (14) is obtained as,

$$F_{\gamma_2}(\gamma_2) \approx \frac{1}{\bar{\gamma}_2\sqrt{2\pi\sigma^2}} \exp\left(-\frac{\mu^2}{2\sigma^2} \right) \sum_{k=0}^{\infty} \frac{1}{k!} \left(\frac{\mu}{\sigma^2\bar{\gamma}_2} \right)^k \times \frac{\gamma_2^{k+1}}{2}\, \mathrm{G}_{2,3}^{1,2}\left[{}^{-\frac{k}{2},\frac{1-k}{2}}_{0,-\frac{(k+1)}{2},-\frac{k}{2}} \middle| \frac{\gamma_2^2}{2\sigma^2\bar{\gamma}_2^2} \right]. \tag{15}$$

3) UWOC LINK

The turbulence of the underwater channel is approximated to the turbulence of free space atmospheric channel and hence it can also be GG distributed [15], [18], [35]. In a strict sense, random air-water interface also plays an important role for underwater wireless optical communications. There is significant reduction in the received communications signal resulting limiting the data transfer capability and the transmitting and in the receiving data rates [36]. The SNR-PDF of the UWOC link is given as [37], [38],

$$f_{\gamma_3}(\gamma_3) = \frac{g_1^2}{r\gamma_3\Gamma(\alpha)\Gamma(\beta)} \mathrm{G}_{1,3}^{3,0}\left[{}^{g_1^2+1}_{g_1^2,\alpha,\beta} \middle| \frac{g_1^2\alpha\beta}{g_1^2+1} \left(\frac{\gamma_3}{\mu_r} \right)^{\frac{1}{r}} \right] \tag{16}$$

where α and β are the underwater turbulence parameters, g_1 represents the pointing error parameter, and r denotes the detection method. When $r = 1$, it is heterodyne detection and if $r = 2$, it is IMDD detection. Since we are considering IMDD detection, the channel PDF for the IMDD detection is given as

$$f_{\gamma_3}(\gamma_3) = \frac{g_1^2}{2\gamma_3\Gamma(\alpha)\Gamma(\beta)} \mathrm{G}_{1,3}^{3,0}\left[{}^{g_1^2+1}_{g_1^2,\alpha,\beta} \middle| \frac{g_1^2\alpha\beta}{g_1^2+1} \left(\frac{\gamma_3}{\mu_2} \right)^{\frac{1}{2}} \right] \tag{17}$$

where

$$\mu_2 = \frac{g_1^2\left(g_1^2+2\right)\bar{\gamma}_3}{\left(g_1^2+1\right)^2\left(1+\frac{1}{\alpha}\right)\left(1+\frac{1}{\beta}\right)}$$

Here $\bar{\gamma}_3$ is the average SNR of the UWOC link. The SNR-CDF of the Eq.17 can be given as

$$F_{\gamma_3}(\gamma_3) = \frac{g_1^2\, 2^{\alpha+\beta-1}}{4\pi\Gamma(\alpha)\Gamma(\beta)} \mathrm{G}_{3,7}^{6,1}\left[{}^{XX}_{YY} \middle| \left(\frac{g_1^2\alpha\beta}{g_1^2+1} \right)^2 \frac{\gamma_3}{16\mu_2} \right] \tag{18}$$

Here

$$XX = \left[1, \frac{g_1^2+1}{2}, \frac{g_1^2+2}{2} \right]$$

and

$$YY = \left[\frac{g_1^2}{2}, \frac{g_1^2+1}{2}, \frac{\alpha}{2}, \frac{\alpha+1}{2}, \frac{\beta}{2}, \frac{\beta+1}{2}, 0 \right].$$

IV. PERFORMANCE EVALUATION

The performance of proposed RIS-assisted triple-hop RF, FSO and UWOC links obtained in terms of outage probability and ABER.

A. OUTAGE PROBABILITY

The probability that blackouts the system's communication when the output SNR drops below a stipulated threshold value is known as Outage Probability (P_{out}). The outage probability of the end-to-end system is given by [39]

$$P_{out} = Pr[\gamma < \gamma_{th}] = F_\gamma(\gamma_{th}) \tag{19}$$

where γ_{th} is the threshold SNR and $F_\gamma(\gamma_{th})$ is the CDF of the triple-hop communication system. The CDF of the end-to-end system considered in Figure 1 is given as

$$F_\gamma(\gamma_{th}) = 1 - \left((1 - F_{\gamma_1}(\gamma_{th}))\,(1 - F_{\gamma_2}(\gamma_{th}))\,(1 - F_{\gamma_3}(\gamma_{th})) \right). \tag{20}$$

After substituting the Eq. (6), (15) and (18) in (19) and by making some mathematical manipulations, the outage probability of the end-to-end system is given in (21), as shown at the bottom of the page.

The asymptotic outage probability of each link obtained using the Eq. (22) of [40] are given as follows.

$$F_{\gamma_1}^{\infty}(\gamma_{th}) \simeq \frac{1}{b^{a+1}\Gamma(a+2)}\left(\frac{\gamma_{th}}{\bar{\gamma_1}}\right)^{\frac{a+1}{2}} \tag{22}$$

$$F_{\gamma_2}^{\infty}(\gamma_{th}) \approx \frac{\exp\left(-\frac{\mu^2}{2\sigma^2}\right)}{\sqrt{2\pi\sigma^2\bar{\gamma}_2^2}}\sum_{k=0}^{\infty}\frac{\gamma_{th}^{k+1}}{(k+1)!}\left(\frac{\mu}{\sigma^2\bar{\gamma}_2}\right)^k \tag{23}$$

$$F_{\gamma_3}^{\infty}(\gamma_{th}) = \sum_{i=1}^{6}\frac{g_1^2(z\gamma_{th})^{YY(i)}}{2^{(3-\alpha-\beta)}\pi\Gamma(\alpha)\Gamma(\beta)} \times\left(\frac{\prod_{j=1,j\neq i}^{6}\Gamma\left(YY(j)-YY(i)\right)\Gamma\left(YY(i)\right)}{\prod_{j=2}^{3}\Gamma\left(XX(j)-YY(i)\right)\Gamma\left(1+YY(i)\right)}\right) \tag{24}$$

where $z = \frac{1}{16\mu_2}\left(\frac{g_1^2\alpha\beta}{g_1^2+1}\right)^2$. Substituting Eqs. (22), (23) and (24) in (20) to gives the asymptotic outage probability of the proposed end-to-end system.

B. ABER CALCULATION

The ABER performance of the system can be evaluated using the ABER of the each individual link. The ABER of the triple-hop system can be given as

$$P_{e2e} = 1 - ((1-P_{e1})(1-P_{e2})(1-P_{e3})) \tag{25}$$

where P_{e1}, P_{e2}, and P_{e3} are the ABER of the RF, FSO, and UWOC links respectively. The ABER of a communication link can be found using the CDF and is given by [10],

$$P_e = \frac{\delta}{2\Gamma(p)}\sum_{K=1}^{\mathscr{K}}\left(q_K^p\int_0^{\infty}\gamma^{p-1}\exp(-q_K\gamma)\,F_{\gamma}(\gamma)d\gamma\right). \tag{26}$$

where p, q and δ represent the type of modulation schemes. Table. 2 shows the values of modulation scheme parameters p and q for ABER calculation.

1) ABER OF THE RF LINK

The ABER of the RIS-assisted RF link can be obtained after substituting Nakagami-m channel CDF Eq. (6) in Eq. (26),

TABLE 1. Turbulence parameter values for the FSO and the UWOC links.

Parameter	FSO Link [4]		UWOC Link [42]	
Turbulence	Strong	Weak	Strong	Weak
C_n^2	3×10^{-12}	5×10^{-14}	10^{-8}	9×10^{-12}
α	11.4336	4.3997	37.7952	4.3790
β	1.0090	2.5717	0.9971	2.5429

TABLE 2. ABER parameters used for binary modulation and M-ary phase shift keying modulation schemes [10].

Modulation Scheme	p	δ	q	$\mathscr{K}$
DBPSK	1	1	1	1
NCBFSK	1	1	0.5	1
CBPSK	0.5	1	1	1
CBFSK	0.5	1	0.5	1
M-PSK	0.5	$\frac{2}{\max(2,\log_2 M)}$	$\sin^2\left(\frac{(2k-1)\pi}{M}\right)$	$\max\left(\frac{M}{4},1\right)$

and performing some mathematical manipulations using the Eq. (22) of Ref. [41] as

$$P_{e1} = \sum_{K=1}^{\mathscr{K}} C_1 \mathrm{G}_{3,4}^{2,3}\left[\begin{matrix}\frac{1}{2},1,1-p\\ \frac{a+1}{2},\frac{a+2}{2},0,\frac{1}{2}\end{matrix}\middle|\frac{1}{4q_K\bar{\gamma_1}b^2}\right] \tag{27}$$

where

$$C_1 = \frac{2^{a-1}\delta}{\Gamma(p)\Gamma(a+1)\sqrt{\pi}}.$$

The asymptotic BER expression of RF link is given as,

$$P_{e1}^{\infty} = \sum_{K=1}^{\mathscr{K}}\frac{\delta\Gamma\left(p+\frac{a+1}{2}\right)}{2\Gamma(p)\left(b\sqrt{q_K\bar{\gamma_1}}\right)^{a+1}\Gamma(a+2)} \tag{28}$$

2) ABER OF THE FSO LINK

The FSO link is also RIS-assisted and its ABER can be found similar to the RF link. The GG channel CDF Eq. (15) is substituted in Eq. (26) and performing calculations using the Eq. (22) of Ref. [41], we get

$$P_{e2} = C_2\sum_{K=1}^{\mathscr{K}}\sum_{k=0}^{\infty}\frac{1}{k!}\left(\frac{\mu}{\sigma^2\bar{\gamma}_2}\right)^k\frac{2^{p+k+\frac{1}{2}}}{q_K^{p+k+1}} \times\mathrm{G}_{4,3}^{1,4}\left[\begin{matrix}-\frac{k}{2},\frac{1-k}{2},-\frac{(p+k)}{2},\frac{1-p-k}{2}\\ 0,-\frac{(k+1)}{2},-\frac{k}{2}\end{matrix}\middle|\frac{1}{2q_K(\sigma\bar{\gamma}_2)^2}\right]. \tag{29}$$

$$F_{\gamma}(\gamma_{th}) = 1-\left(1-\frac{1}{\Gamma(a+1)}\mathrm{G}_{1,2}^{1,1}\left[\begin{matrix}1\\ a+1,0\end{matrix}\middle|\frac{1}{b}\sqrt{\frac{\gamma_{th}}{\bar{\gamma_1}}}\right]\right) \times\left(1-\frac{1}{\bar{\gamma}_2\sqrt{2\pi\sigma^2}}\exp\left(-\frac{\mu^2}{2\sigma^2}\right)\sum_{k=0}^{\infty}\frac{1}{k!}\left(\frac{\mu}{\sigma^2\bar{\gamma}_2}\right)^k\frac{\gamma_{th}^{k+1}}{2}\mathrm{G}_{2,3}^{1,2}\left[\begin{matrix}-\frac{k}{2},\frac{1-k}{2}\\ 0,-\frac{(k+1)}{2},-\frac{k}{2}\end{matrix}\middle|\frac{\gamma_{th}^2}{2\sigma^2\bar{\gamma}_2^2}\right]\right) \times\left(1-\frac{g_1^2\,2^{\alpha+\beta-1}}{4\pi\Gamma(\alpha)\Gamma(\beta)}\mathrm{G}_{3,7}^{6,1}\left[\begin{matrix}XX\\ YY\end{matrix}\middle|\left(\frac{g_1^2\alpha\beta}{g_1^2+1}\right)^2\frac{\gamma_{th}}{16\mu_2}\right]\right) \tag{21}$$

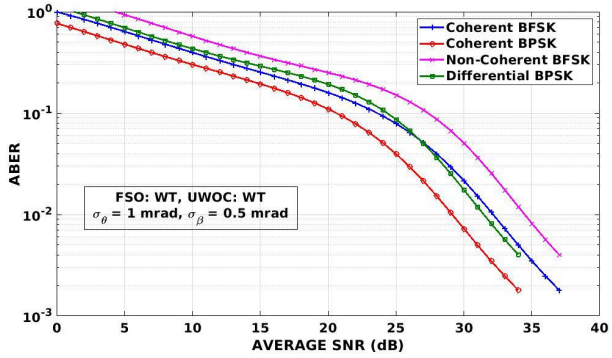

FIGURE 2. ABER performance of triple-hop system for different modulation schemes.

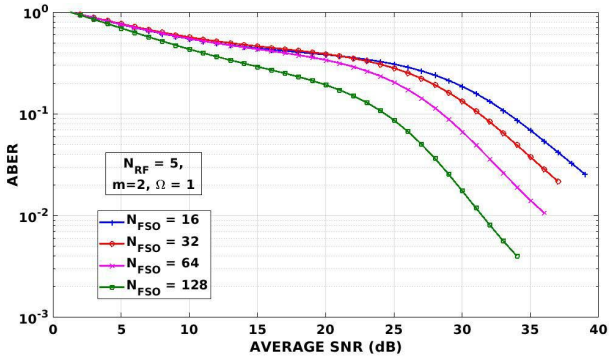

FIGURE 3. ABER performance of end-to-end system for varying N_{FSO}.

where

$$C_2 = \frac{\delta q_K^p}{8\pi\Gamma(p)\sigma\bar{\gamma}_2}\exp\left(-\frac{\mu^2}{2\sigma^2}\right).$$

The asymptotic BER expression of FSO link is given as,

$$P_{e2}^{\infty} = \frac{\delta\exp\left(-\frac{\mu^2}{2\sigma^2}\right)}{2\Gamma(p)\sqrt{2\pi\sigma^2\bar{\gamma}_2^2}}\sum_{K=1}^{\mathcal{K}}\sum_{k=0}^{\infty}\frac{\Gamma(p+k+1)}{q_K^{(k+2)}(k+1)!}\left(\frac{\mu}{\sigma^2\bar{\gamma}_2}\right)^k \tag{30}$$

3) ABER OF THE UWOC LINK

The ABER of the UWOC link can be calculated after substituting Eq. (18) in Eq. (26) and using the Eq. (22) of Ref. [41] as

$$P_{e3} = \sum_{K=1}^{\mathcal{K}} C_3\, \mathrm{G}_{4,7}^{6,2}\left[\begin{matrix} XX, 1-p \\ YY \end{matrix}\middle|\left(\frac{g_1^2\alpha\beta}{g_1^2+1}\right)^2\frac{1}{16q_K\mu_2}\right] \tag{31}$$

where

$$C_3 = \frac{\delta g_1^2 2^{\alpha+\beta-2}}{4\pi\Gamma(p)\Gamma(\alpha)\Gamma(\beta)}$$

The asymptotic BER expression of the UWOC system is given in Eq. (32), as shown at the bottom of the next page.

The ABER of the end-to-end triple-hop system can be calculated after substituting the Eqs. (27), (29), and (31) in (25) is given in (33), as shown at the bottom of the next page. Similarly, the end-to-end asymptotic ABER obtained by substituting Eqs. (28), (30) and (32) in (25).

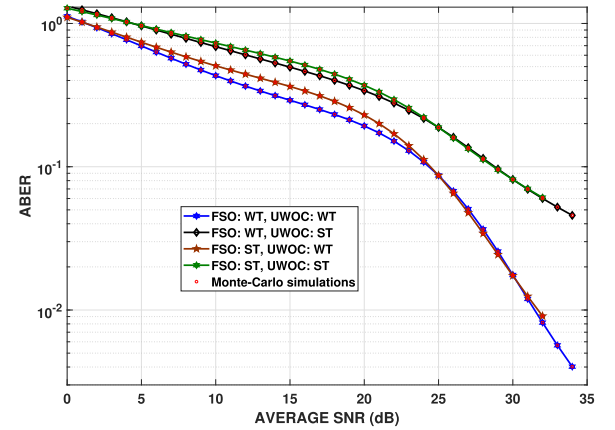

FIGURE 4. Analytical and Monte-Carlo simulation ABER performance of triple-hop convergent system for varying turbulence.

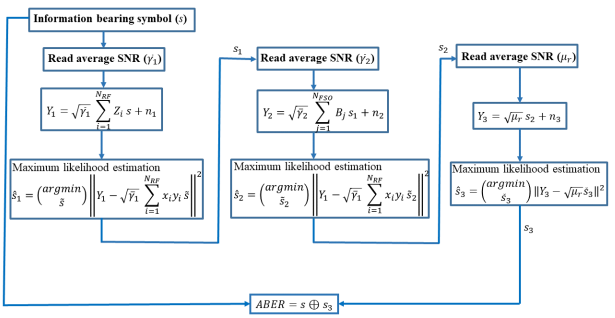

FIGURE 5. Flowchart of ABER Monte-Carlo simulations.

V. RESULTS AND DISCUSSIONS

This section provides the numerical results to explain the ABER and outage probability performance of the RIS-assisted triple-hop RF-FSO convergent with the UWOC system. We observed the impact of the essential system parameters on the system performance. The RIS-RF link parameters are considered as $N_{RF} = 5$, $m = 2$, $\Omega = 1$. a_r, w_z, σ_θ, and σ_β values are used to calculate the pointing error parameter value of the RIS-FSO link. We considered weak misalignment fading for the UWOC link. Calculated the turbulence parameters α and β of RIS-FSO and UWOC links using σ_R^2. We used different refractive index structure constants for the FSO (C_n^2 range from 10^{-12} to 10^{-17}) and UWOC (C_n^2 range from 10^{-8} to 10^{-14}) channels. The wavelength of $\lambda = 1550$ nm and $\lambda = 530$ nm are used for the FSO and the UWOC links, respectively. The direct link range is 30 m for the UWOC link throughout all the results. Table. 1 gives the α and β parameters for different C_n^2 values.

Figures 2 to 8 show the ABER performances and figures 9 to 12 depict the outage probability performance with respect to average SNR of the triple-hop communication system. Figure 2 shows the performance of the end-to-end system

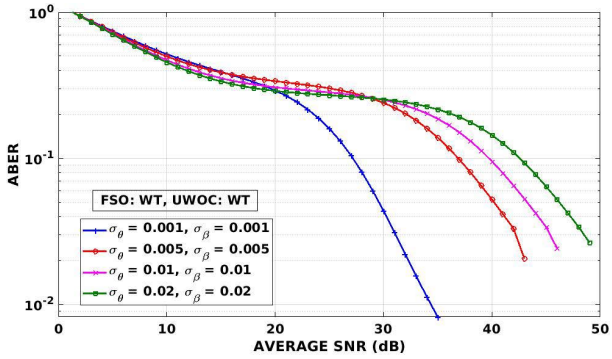

FIGURE 6. ABER performance of end-to-end system for varying σ_θ and σ_β values when $N_{FSO} = 128$ and $L_1 = L_2 = 500$ m.

for various modulation schemes, namely differential binary phases shift keying (DBPSK), non-coherent binary frequency shift keying (NCBFSK), coherent binary phases shift keying (CBPSK), and coherent binary frequency shift keying (CBFSK). CBPSK, DBPSK, CBFSK and NCBFSK modulation schemes obtains 4×10^{-3} ABER performance at 31.75, 34, 34.50 and 37 dB, respectively. From the ABER results, CBPSK performs 2.25 dB, 2.75 dB and 7.25 dB superior from DBPSK, CBFSK and NCBFSK modulation schemes at 4×10^{-3} ABER, respectively. The ABER of the triple-hop communication system was analyzed for $\sigma_\theta = 1$ mrad, $\sigma_\beta = 0.5$ mrad, $a_r = 0.1$, $w_z = 1.2$, $N_{FSO} = 128$, $L_1 = L_2 = 500$ m, and weak turbulence over the FSO and the UWOC links. We observed that the Coherent BPSK scheme gives better ABER performance than other modulation schemes.

Figure 3 presents the ABER performance for the varying N_{FSO} values. We considered 16, 32, 64, and 128 as the N_{FSO} values and $\sigma_\theta = 1$ mrad, $\sigma_\beta = 0.5$ mrad. Weak turbulence is considered for the FSO and the UWOC links along with $a_r = 0.1$, $w_z = 1.2$, $L_1 = L_2 = 500$ m. As N_{FSO} value increases there is an improvement in the performance of the end-to-end system. Using the same values, except turbulence, making N_{FSO} as 128, the Figure 4 portrays the ABER performance of analytical and Monte-Carlo simulations in terms of average SNR. The turbulence of the FSO and the UWOC links varied. The ABER performance of weak and strong turbulence influenced systems for the FSO and UWOC attains at 27 and 34 dB at 4×10^{-2} ABER, respectively. Hence the strong turbulence influenced FSO and UWOC systems deteriorates 7 dB ABER performance when compared with the weak turbulence influenced FSO and UWOC system. Figure 5 shows the flowchart Monte-Carlo simulations carried for the proposed end-to-end communication system. In figure 5, $\hat{s}$ indicates the estimated data, $\tilde{s}$ means the symbol of specific modulation.

Figure 6 depicts the end-to-end system's ABER performance for varying the standard deviations of pointing errors and deflection error angles *i.e.*, σ_θ and σ_β, respectively. Since these values are used to calculate the pointing error parameter of the FSO link, they are considered in the system's performance. Along with weak turbulence on the FSO and the UWOC links, $a_r = 0.1$, $w_z = 1.2$, are considered. The σ_θ and σ_β values are considered as 1 mrad for very weak pointing errors, 5 mrad for weak pointing errors, 10 mrad for moderate pointing errors, and 20 mrad for strong pointing errors. The very weak pointing error influenced system attains 2.5×10^{-2} ABER performance at 31.75 dB, where as weak, moderate and strong pointing error influenced triple-hop communication systems obtain the same ABER performance at 42.50 dB, 46 dB and 49 dB, respectively. Hence, the standard deviation of pointing error and deflection angle error values increase, the ABER performance deteriorates, i.e., the end-to-end system's performance degraded.

With the values $a_r = 0.1$ and $w_z = 1.2$, the turbulence of one link is considered as constant and varied the turbulence of other link and σ_θ of the FSO link in Figure 7. Figure 7a shows the ABER performance for the varying turbulence of the FSO link. There is a remarkable change in the ABER with varying σ_θ. When $\sigma_\theta = 1$ mrad, we observe the degradation in the system performance compared to the $\sigma_\theta = 0.1$ mrad. It shows the pointing error effect of the FSO link on the end-to-end system. There is a small degradation in the system performance with a change in the turbulence of the FSO link. Similar to this, Figure 7b presents the ABER performance

$$P_{e3}^{\infty} = \frac{\delta g_1^2 \, 2^{\alpha+\beta-1}}{8\pi\Gamma(p)\Gamma(\alpha)\Gamma(\beta)} \sum_{K=1}^{\mathcal{K}} \sum_{i=1}^{6} \left(\frac{z}{q_K}\right)^{YY(i)} \left(\frac{\prod_{j=1, j\neq i}^{6} \Gamma\left(YY(j) - YY(i)\right) \Gamma\left(YY(i)\right) \Gamma(p + YY(i))}{\prod_{j=2}^{3} \Gamma\left(XX(j) - YY(i)\right) \Gamma\left(1 + YY(i)\right)}\right) \tag{32}$$

$$\begin{aligned} P_{e2e} = 1 - \sum_{K=1}^{\mathcal{K}} & \left(1 - C_1 \, \mathrm{G}_{3,4}^{2,3}\left[\begin{matrix} \frac{1}{2}, 1, 1-p \\ \frac{a+1}{2}, \frac{a+2}{2}, 0, \frac{1}{2} \end{matrix} \middle| \frac{1}{4q_K \bar{\gamma}_1 b^2}\right]\right) \\ & \times \left(1 - C_2 \sum_{k=0}^{\infty} \frac{1}{k!} \left(\frac{\mu}{\sigma^2 \bar{\gamma}_2}\right)^k \frac{2^{p+k+\frac{1}{2}}}{q_K^{p+k+1}} \, \mathrm{G}_{4,3}^{1,4}\left[\begin{matrix} -\frac{k}{2}, \frac{1-k}{2}, -\frac{(p+k)}{2}, \frac{1-p-k}{2} \\ 0, -\frac{(k+1)}{2}, -\frac{k}{2} \end{matrix} \middle| \frac{1}{2q_K (\sigma \bar{\gamma}_2)^2}\right]\right) \\ & \times \left(1 - C_3 \, \mathrm{G}_{4,7}^{6,2}\left[\begin{matrix} XX, 1-p \\ YY \end{matrix} \middle| \left(\frac{g_1^2 \alpha\beta}{g_1^2 + 1}\right)^2 \frac{1}{16 q_K \mu_2}\right]\right) \end{aligned} \tag{33}$$

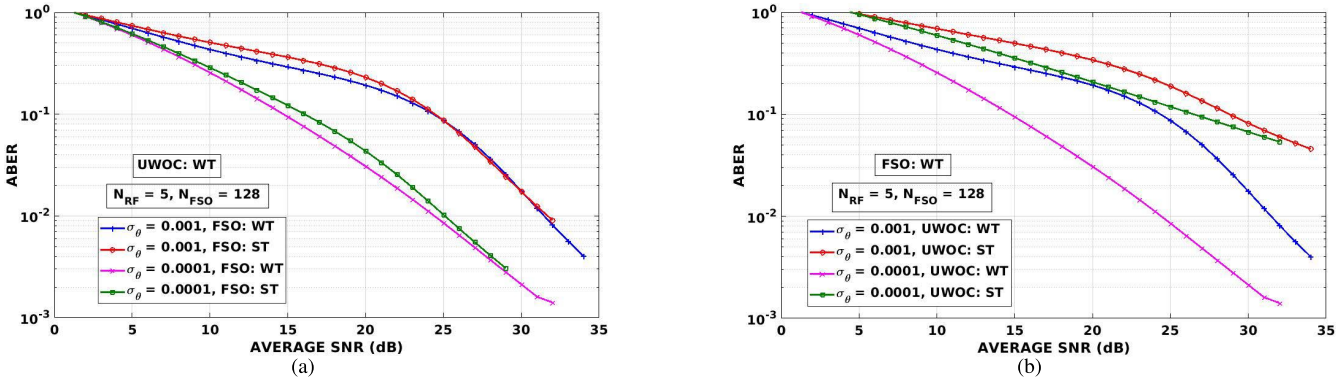

FIGURE 7. ABER performance for varying σ_θ and turbulence values (a) for varying FSO turbulence & (b) for varying UWOC turbulence.

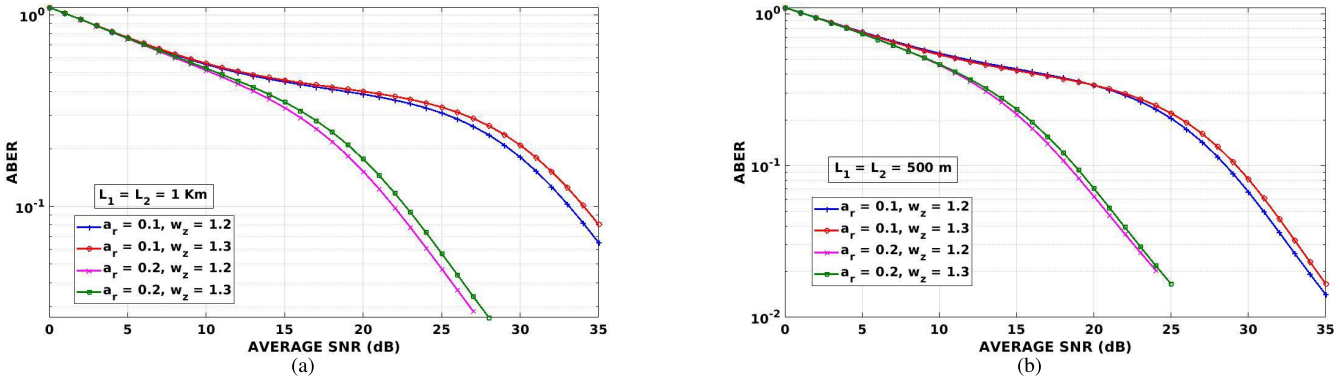

FIGURE 8. ABER performance for varying a_r and w_z values over different link distances from RIS to source/destination/relay (a) for 1 Km link & (b) for 500 m link.

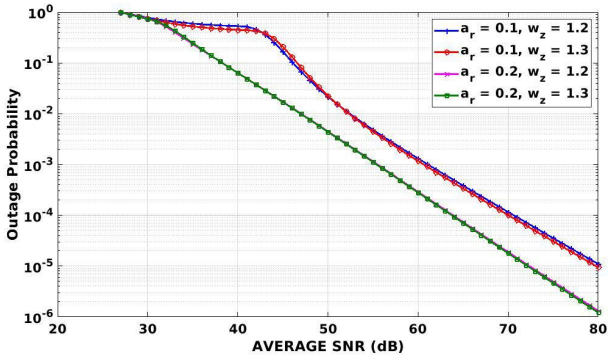

FIGURE 9. Outage probability performance of triple-hop communication system for varying a_r and w_z values.

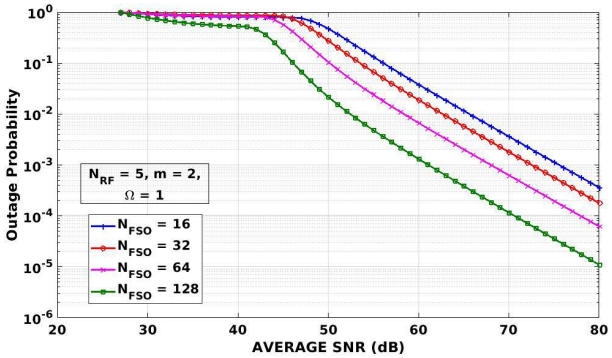

FIGURE 10. Outage probability performance of end-to-end system for varying N_{FSO}.

of the end-to-end system for the varying turbulence of the UWOC link by assuming weak turbulence on the FSO link. There is a significant deviation in the ABER from weak turbulence to strong turbulence of the UWOC link. At 30 dB of average SNR, when $\sigma_\theta = 0.1$ mrad, for the weak turbulence case, ABER is about 10^{-3} and for the strong turbulence case, ABER is less than 10^{-2}.

Figure 8 displays the ABER analysis for the 1Km and 500m FSO links. We considered N_{FSO} as 64 and weak turbulence in both the FSO and UWOC links. There is a degradation in the ABER performance when the beam width w_z for the same value of a_r. We observe an improvement in the system performance with the increase in a_r value. When compared to the system performance of the 1 Km FSO link (Figure 8a), ABER is better for the 500 m of the FSO link (Figure 8b). It shows that, as link length increases, performance decreases.

The outage probability is another performance parameter shown in figures 9 to 12. Similar to ABER, to get all the

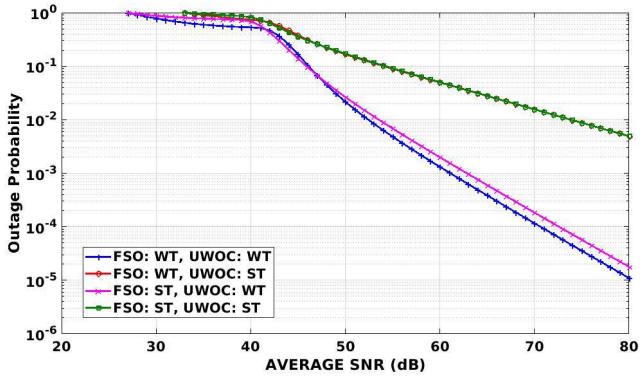

FIGURE 11. Outage performance of the triple-hop convergent system for varying turbulence.

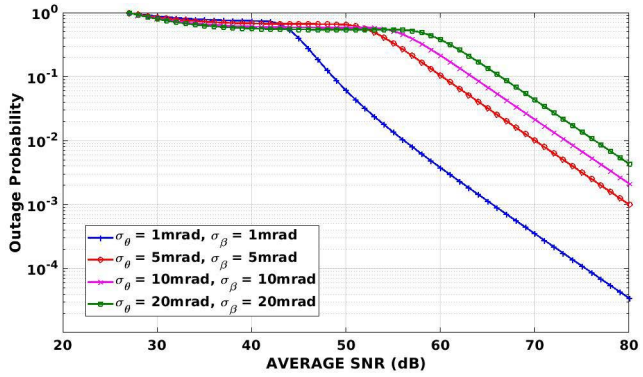

FIGURE 12. Outage performance of end-to-end system for varying σ_θ and σ_β values.

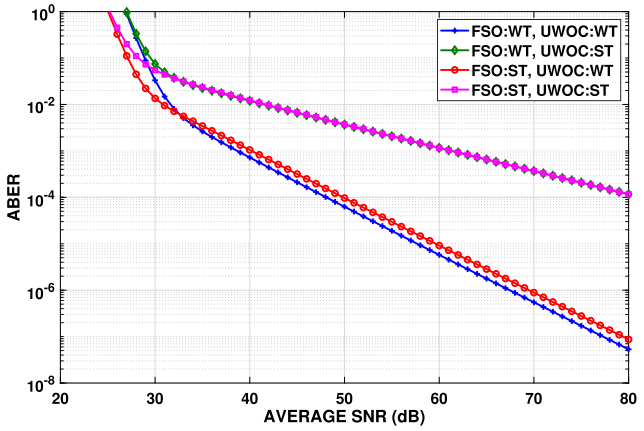

FIGURE 13. Asymptotic analysis of ABER over average SNR of triple-hop communication system for varying turbulence.

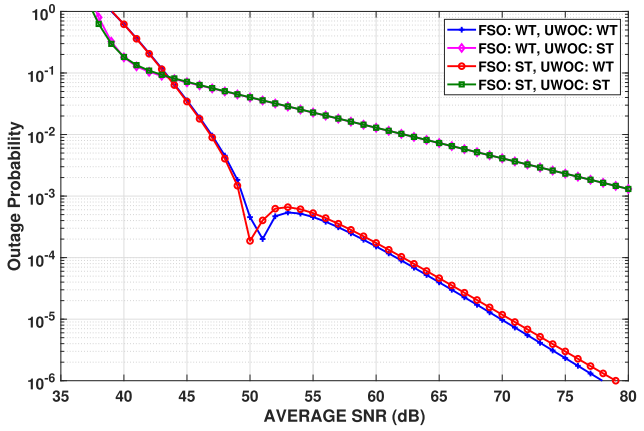

FIGURE 14. Asymptotic analysis of outage probability over average SNR of triple-hop communication system for varying turbulence.

outage results, we considered RF link parameters $N_{RF} = 5$, $m = 2$, $\Omega = 1$. The FSO link lengths L_1 and L_2 considered as 500 m. Figure 9 shows the outage performance of the end-to-end system for the varying a_r and w_z values. We considered weak turbulence over both the FSO and the UWOC links. There is a significant improvement in the outage of the system when the a_r value increase. At 60 dB of average SNR, the outage is approximately 10^{-3} when $a_r = 0.1$ and it is greater than 10^{-3} when $a_r = 0.2$.

Figure 10 depicts the outage performance for varying N_{FSO} of the FSO link when the turbulence is weak for FSO and UWOC links. We considered $\sigma_\theta = 1$ mrad, and $\sigma_\beta = 0.5$ mrad. We notice that the outage is increasing with the increase in the N_{FSO} value.

Figure 11 portrays the triple-hop system's outage performance for varying turbulence of the FSO and the UWOC links. For this we considered $N_{FSO} = 128$, $\sigma_\theta = 1$ mrad, and $\sigma_\beta = 0.5$ mrad. When one link turbulence is made constant, another link turbulence varied. Compared to the FSO link, the UWOC link's turbulence shows significant changes from weak turbulence to strong turbulence cases. At 70 dB of average SNR, when the FSO link has weak turbulence, the outage is at 10^{-4} for weak turbulence of the UWOC link, and it is approximately at 10^{-2}.

Figure 12 shows the outage performance for the varying σ_θ and σ_β values of the FSO link. These parameters are pointing error-related and make notable changes in the end-to-end system performance; as these values increase from 1 mrad to 20 mrad, the outage performance decrease. Hence the effect of the pointing error of the FSO link is larger on the end-to-end system performance.

Asymptotic outage probability and ABER performance of the proposed system are shown in Figures 13 and 14, respectively for the varying turbulence regimes from the weak to strong. From Figures 4 and 13, ABER asymptotic analysis matches with the exact analysis after an average SNR of 30 dB. Similarly, from Figures 11 and 14, the slope of asymptotic outage performance of matches with the exact analysis around around 60 dB average SNR.

At high SNR regime, outage probability as a function of coding and diversity gain is given as $P_{out} \approx (G_c\gamma)^{-G_d}$, where G_c is coding gain and G_d is diversity gain [43]. For the un-coded system $G_c = 1$, and diversity gain is given as $G_d = \frac{\ln \gamma}{\ln (P_{out})}$. Figure 15 shows the diversity gain analysis obtained from asymptotic outage performance (P_{out}) for the varying

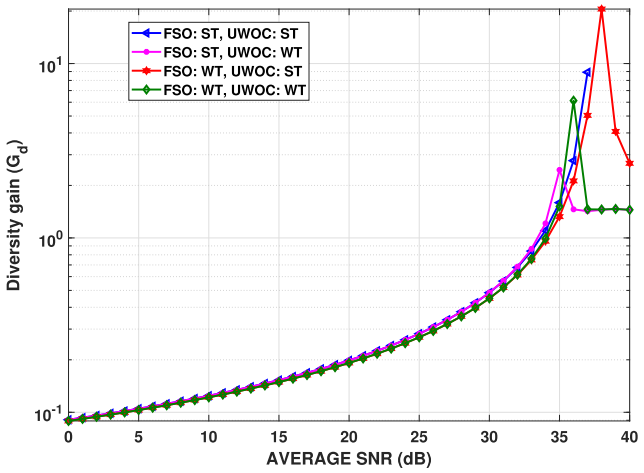

FIGURE 15. Diversity gain analysis over average SNR of triple-hop communication system for varying turbulence.

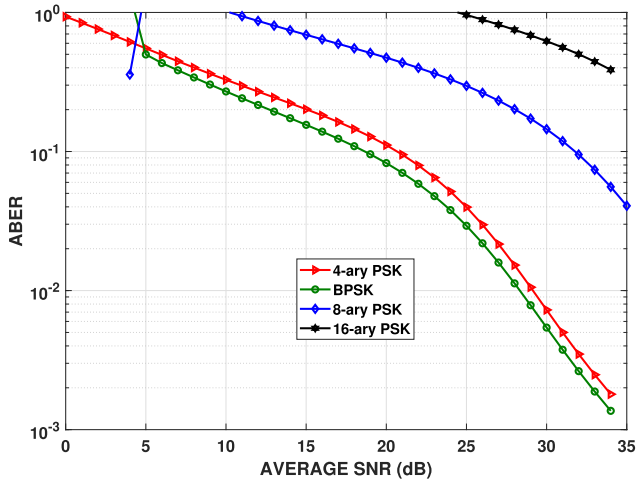

FIGURE 16. ABER comparison of various M-PSK modulation schemes.

weak and strong turbulence regimes of FSO-UWOC links with respect to average SNR. Diversity gain (G_d) at 36 dB average SNR is 9, 1.6, 2.2 and 6 for FSO and UWOC links turbulence are varying ST-ST, ST-WT, WT-ST and WT-WT, respectively.

ABER comparison proposed system for the varying M-PSK modulation schemes under the influence of weak FSO and UWOC turbulence regimes is shown in Figure 16. From figure, increasing the modulation ary deteriorates the system ABER performance, this is due to the number of information bits are increases with the increase in M-ary PSK size.

VI. CONCLUSION

This paper proposed and investigated a triple-hop RIS-assisted RF-FSO convergent with the UWOC system for skip-zones in specific areas. We derived closed-form expressions for ABER and the outage probability under the misalignment fading and turbulence conditions. The results indicate that deploying RISs can significantly improve the end-to-end system's performance. Additionally, the results demonstrate the effect of link distance, turbulence, pointing error, and RIS surface elements on system performance. The ABER and outage probability of the system are significantly improved for weak turbulence, weak misalignment fading, and an increasing number of RIS elements.

REFERENCES

[1] Z. Ghassemlooy, W. Popoola, and S. Rajbhandari, *Optical Wireless Communications: System and Channel Modelling With MATLAB*. Boca Raton, FL, USA: CRC Press, 2019.

[2] A. K. Majumdar, *Advanced Free Space Optics (FSO): A Systems Approach*, vol. 186. New York, NY, USA: Springer, 2014.

[3] A. Sikri, A. Mathur, P. Saxena, M. R. Bhatnagar, and G. Kaddoum, "Reconfigurable intelligent surface for mixed FSO-RF systems with co-channel interference," *IEEE Commun. Lett.*, vol. 25, no. 5, pp. 1605–1609, May 2021.

[4] A. R. Ndjiongue, T. M. N. Ngatched, O. A. Dobre, A. G. Armada, and H. Haas, "Performance analysis of RIS-based nT-FSO link over G-G turbulence with pointing errors," 2021, *arXiv:2102.03654*.

[5] L. Yang, W. Guo, D. B. da Costa, and M.-S. Alouini, "Free-space optical communication with reconfigurable intelligent surfaces," 2020, *arXiv:2012.00547*.

[6] J. Vellakudiyan, V. Palliyembil, I. S. Ansari, P. Muthuchidambaranathan, and K. A. Qaraqe, "Performance analysis of the decode- and-forward relay-based RF-FSO communication system in the presence of pointing errors," *IET Signal Process.*, vol. 13, no. 4, pp. 480–485, Jun. 2019.

[7] W. M. R. Shakir and M.-S. Alouini, "Secrecy performance analysis of parallel FSO/mm-wave system over unified Fisher-snedecor channels," *IEEE Photon. J.*, vol. 14, no. 2, pp. 1–13, Apr. 2022.

[8] S. C. Tokgoz, S. Althunibat, S. L. Miller, and K. A. Qaraqe, "On the secrecy capacity of hybrid FSO-mmWave wiretap channels," *IEEE Trans. Veh. Technol.*, vol. 71, no. 4, pp. 4073–4086, Apr. 2022.

[9] Y. Zhang, J. Zhang, L. Yang, B. Ai, and M.-S. Alouini, "On the performance of dual-hop systems over mixed FSO/mmWave fading channels," *IEEE Open J. Commun. Soc.*, vol. 1, pp. 477–489, 2020.

[10] P. N. Ramavath, S. A. Udupi, and P. Krishnan, "Co-operative RF-UWOC link performance over hyperbolic tangent log-normal distribution channel with pointing errors," *Opt. Commun.*, vol. 469, Aug. 2020, Art. no. 125774.

[11] S. Anees and R. Deka, "On the performance of DF based dual-hop mixed RF/UWOC system," in *2019 IEEE 89th Veh. Technol. Conf. (VTC-Spring)*, Apr./May 2019, pp. 1–5.

[12] R. P. Naik, G. G. Simha, and P. Krishnan, "Wireless-optical-communication-based cooperative IoT and IoUT system for ocean monitoring applications," *Appl. Opt.*, vol. 60, no. 29, pp. 9067–9073, 2021.

[13] A. Jurado-Navas, J. M. Garrido-Balsells, M. Castillo-Vázquez, A. García-Zambrana, and A. Puerta-Notario, "Converging underwater and FSO ground communication links," in *Proc. Opt. Fiber Commun. Conf. Exhib. (OFC)*, 2019, pp. 1–3.

[14] C. Christopoulou, H. G. Sandalidis, and I. S. Ansari, "Outage probability of a multisensor mixed UOWC–FSO setup," *IEEE Sensors Lett.*, vol. 3, no. 8, pp. 1–4, Aug. 2019.

[15] B. K. Levidala and P. Krishnan, "Asymptotic bit error rate analysis of convergent underwater wireless optical communication-free-space optical system over combined channel model for different turbulence and weather conditions with pointing errors," *Opt. Eng.*, vol. 59, no. 11, Nov. 2020, Art. no. 116102.

[16] B. K. Levidala, P. N. Ramavath, and P. Krishnan, "Performance enhancement using multiple input multiple output in dual-hop convergent underwater wireless optical communication–free-space optical communication system under strong turbulence with pointing errors," *Opt. Eng.*, vol. 60, no. 10, Oct. 2021, Art. no. 106106.

[17] L. Yang, Q. Zhu, S. Li, I. S. Ansari, and S. Yu, "On the performance of mixed FSO-UWOC dual-hop transmission systems," *IEEE Wireless Commun. Lett.*, vol. 10, no. 9, pp. 2041–2045, Sep. 2021.

[18] L. B. Kumar and P. Krishnan, "Multi-hop convergent FSO-UWOC system to establish a reliable communication link between the islands," *Opt. Commun.*, vol. 474, Nov. 2020, Art. no. 126107.

[19] M. A. Esmail, A. M. Ragheb, H. A. Fathallah, M. Altamimi, and S. A. Alshebeili, "5G-28 GHz signal transmission over hybrid all-optical FSO/RF link in dusty weather conditions," *IEEE Access*, vol. 7, pp. 24404–24410, 2019.
[20] W.-S. Tsai, C.-Y. Li, H.-H. Lu, Y.-F. Lu, S.-C. Tu, and Y.-C. Huang, "256 Gb/s four-channel SDM-based PAM4 FSO-UWOC convergent system," *IEEE Photon. J.*, vol. 11, no. 2, pp. 1–8, Apr. 2019.
[21] W.-S. Tsai, H.-H. Lu, H.-W. Wu, S.-C. Tu, Y.-C. Huang, J.-Y. Xie, Q.-P. Huang, and S.-E. Tsai, "500 Gb/s PAM4 FSO-UWOC convergent system with a R/G/B five-wavelength polarization-multiplexing scheme," *IEEE Access*, vol. 8, pp. 16913–16921, 2020.
[22] C.-Y. Li, H.-H. Lu, Y.-C. Wang, Z.-H. Wang, C.-W. Su, Y.-F. Lu, and W.-S. Tsai, "An 82-m 9 Gb/s PAM4 FSO-POF-UWOC convergent system," *IEEE Photon. J.*, vol. 11, no. 1, pp. 1–9, Feb. 2019.
[23] Y. Liu, X. Liu, X. Mu, T. Hou, J. Xu, M. Di Renzo, and N. Al-Dhahir, "Reconfigurable intelligent surfaces: Principles and opportunities," *IEEE Commun. Surveys Tuts.*, vol. 23, no. 3, pp. 1546–1577, 3rd Quart., 2021.
[24] L. Yang, F. Meng, J. Zhang, M. O. Hasna, and M. D. Renzo, "On the performance of RIS-assisted dual-hop UAV communication systems," *IEEE Trans. Veh. Technol.*, vol. 69, no. 9, pp. 10385–10390, Sep. 2020.
[25] I. Yildirim, A. Uyrus, and E. Basar, "Modeling and analysis of reconfigurable intelligent surfaces for indoor and outdoor applications in future wireless networks," *IEEE Trans. Commun.*, vol. 69, no. 2, pp. 1290–1301, Feb. 2021.
[26] H. Wang, Z. Zhang, B. Zhu, J. Dang, L. Wu, L. Wang, K. Zhang, Y. Zhang, and G. Y. Li, "Performance analysis of multi-branch reconfigurable intelligent surfaces-assisted optical wireless communication system in environment with obstacles," *IEEE Trans. Veh. Technol.*, vol. 70, no. 10, pp. 9986–10001, Oct. 2021.
[27] L. Yang, W. Guo, and I. S. Ansari, "Mixed dual-hop FSO-RF communication systems through reconfigurable intelligent surface," *IEEE Commun. Lett.*, vol. 24, no. 7, pp. 1558–1562, Jul. 2020.
[28] S. Li, L. Yang, D. B. D. Costa, M. D. Renzo, and M.-S. Alouini, "On the performance of RIS-assisted dual-hop mixed RF-UWOC systems," *IEEE Trans. Cogn. Commun. Netw.*, vol. 7, no. 2, pp. 340–353, Jun. 2021.
[29] M. Najafi and R. Schober, "Intelligent reflecting surfaces for free space optical communications," in *Proc. IEEE Global Commun. Conf. (GLOBECOM)*, Dec. 2019, pp. 1–7.
[30] A. M. Abdelhady, A. K. S. Salem, O. Amin, B. Shihada, and M.-S. Alouini, "Visible light communications via intelligent reflecting surfaces: Metasurfaces vs mirror arrays," *IEEE Open J. Commun. Soc.*, vol. 2, pp. 1–20, 2020.
[31] M. Najafi, B. Schmauss, and R. Schober, "Intelligent reflecting surfaces for free space optical communication systems," *IEEE Trans. Commun.*, vol. 69, no. 9, pp. 6134–6151, Sep. 2021.
[32] M. H. Samuh, A. M. Salhab, and A. H. A. El-Malek, "Performance analysis and optimization of RIS-assisted networks in Nakagami-m environment," 2020, *arXiv:2010.07841*.
[33] A. P. Prudnikov, I. A. Brychkov, and O. I. Marichev, *Integrals and Series: More Special Functions: V.3*. New York, NY, USA: Gordon and Breach, 1986.
[34] I. S. Gradshteyn and I. M. Ryzhik, *Table of Integrals, Series, and Products*. New York, NY, USA: Academic, 2014.
[35] Y. Fu and Y. Du, "Performance of heterodyne differential phase-shift-keying underwater wireless optical communication systems in gamma-gamma-distributed turbulence," *Appl. Opt.*, vol. 57, no. 9, pp. 2057–2063, Mar. 2018.
[36] A. K. Majumdar, J. Siegenthaler, and P. Land, "Analysis of optical communications through the random air-water interface: Feasibility for under-water communications," *Proc. SPIE*, vol. 8517, Oct. 2012, Art. no. 85170T.
[37] L. B. Kumar, P. N. Ramavath, P. Krishnan, and A. K. Majumdar, "Underwater wireless optical communications based reconfigurable UOWSN for monitoring and discovering continental margin ore deposits," *Appl. Opt.*, vol. 61, no. 11, pp. 3141–3149, 2022.
[38] I. S. Ansari, F. Yilmaz, and M.-S. Alouini, "Performance analysis of free-space optical links over Málaga ($\mathcal{M}$) turbulence channels with pointing errors," *IEEE Trans. Wireless Commun.*, vol. 15, no. 1, pp. 91–102, Jan. 2016.
[39] K. Prabu, D. S. Kumar, and T. Srinivas, "Performance analysis of FSO links under strong atmospheric turbulence conditions using various modulation schemes," *Optik*, vol. 125, no. 19, pp. 5573–5581, Oct. 2014.
[40] P. N. Ramavath and W.-Y. Chung, "Evaluation of reconfigurable intelligent surface-assisted underwater wireless optical communication system," *J. Lightw. Technol.*, early access, Mar. 31, 2022, doi: 10.1109/JLT.2022.3162627.
[41] V. S. Adamchik and O. I. Marichev, "The algorithm for calculating integrals of hypergeometric type functions and its realization in REDUCE system," in *Proc. Int. Symp. Symbolic Algebr. Comput.*, 1990, pp. 212–224.
[42] W. Liu, Z. Xu, and L. Yang, "SIMO detection schemes for underwater optical wireless communication under turbulence," *Photon. Res.*, vol. 3, no. 3, pp. 48–53, Oct. 2015.
[43] H. Ding, J. Ge, D. B. da Costa, and Z. Jiang, "Asymptotic analysis of cooperative diversity systems with relay selection in a spectrum-sharing scenario," *IEEE Trans. Veh. Technol.*, vol. 60, no. 2, pp. 457–472, Feb. 2011.

L. BHARGAVA KUMAR received the master's degree from Jawaharlal Nehru Technological University Anantapur, Andhra Pradesh, India. He is currently pursuing the Ph.D. degree with the National Institute of Technology Karnataka, Surathkal, India. His research interests include optical and wireless communication, free-space optical communication, and underwater optical wireless communication.

RAMAVATH PRASAD NAIK received the M.Tech. degree from the Department of Electronics and Communication Engineering, Motilal Nehru National Institute of Technology Allahabad, in 2015, and the Ph.D. degree from the National Institute of Technology Karnataka, Surathkal, in 2021. He is currently working as a Postdoctoral Researcher with the Research Institute of Artificial Intelligence Convergence, Pukyong National University, Busan, Republic of Korea. His research interests include free-space and underwater optical wireless communication, theory and application of error control codes, and co-operative communication.

PRABU KRISHNAN (Senior Member, IEEE) received the Ph.D. degree in free space optical communication from the Department of Electronics and Communication Engineering, NIT, Trichy, India. He is currently working as an Assistant Professor with the Department of Electronics and Communication Engineering, NITK, Surathkal, India. He has been recognized as one of the world's top 2% researchers for the years 2019 and 2020. His research interests include optical wireless communications, radio over free space optical communications, radio over fiber, optical sensors, and nano-photonics.

A. AROCKIA BAZIL RAJ (Member, IEEE) has been working with the Department of Electronics Engineering, DIAT, since 2015. Before DIAT, he was with the Research Development and Establishment (RDE) Section, DRDO Laser Communication Research Facility, since 2007. He has 16 years of research/academic/consultancy work experience and demonstrated his competency in creating technology for several requirements of government/private sectors/industries. His Ph.D. research on communication and signal processing was fully funded by the DRDO, New Delhi, India. He has delivered several invited talks and headed national/international conference sessions. He has completed/investigated various research and consultancy projects sponsored by government and non-government sectors/laboratories/industries. His research interests include high-performance digital system design in FPGA, real-time digital/optical signal processing, radar system design, radar signal processing, LSS targets imaging, free space optical communication and free space QKD, and RF photonics.

ARUN K. MAJUMDAR (Life Member, IEEE) has over 30 years of professional expertise and has demonstrated leadership skills in research and development from within industry, university and national laboratory settings in the areas of atmospheric turbulence effects on free-space laser communications, propagation, and imaging. He has led seminars and short courses at various organizations throughout the world, such as The Boeing Company (USA), BAE Systems (USA), Gujrat University (India), and Oxford University (U.K.) to name just a few. His current research interests include free-space laser communications, advanced FSO communications, and image corrections and communications through atmospheric turbulence.

WAN-YOUNG CHUNG (Senior Member, IEEE) received the B.Eng. and master's degrees in electronic engineering from Kyungpook National University, Daegu, South Korea, in 1987 and 1989, respectively, and the Ph.D. degree in sensor engineering from Kyushu University, Fukuoka, Japan, in 1998. From 1999 to 2008, he was an Associate Professor at Dongseo University, Busan, South Korea. He is currently a Professor with the Department of Electronic Engineering, Pukyong National University, Busan. He is the Educational and Research Group Leader for artificial intelligence convergence, which is supported by the Brain Korea 21 (BK21) Four Project. His research interests include wireless sensor networks, ubiquitous healthcare and automobile applications, smart light-emitting systems with visible light communication, and embedded systems.